Available online at www.sciencedirect.com

ScienceDirect

journal homepage: www.elsevier.com/locate/he

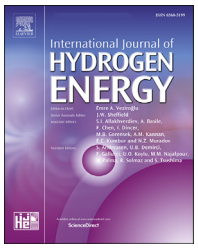

Efficient recovery of syngas from dry methane reforming product by a dual pressure swing adsorption process

José Antonio Delgado Dobladez[*], *Vicente Ismael Águeda Maté*, *Silvia Álvarez Torrellas*, *Marcos Larriba*, *Pablo Brea*

Department of Chemical Engineering, Universidad Complutense de Madrid, 28040 Madrid, Spain

HIGHLIGHTS

- Dual PSA has been designed to recover syngas from a dry methane reforming product.
- Syngas recovered with purity and recovery >99%.
- Conversion at 700 °C raised to 100%.
- SEI = 4.7 kJ/L thermal is lower than that of plasma reactors.
- Syngas from tail gas of H_2 PSA can also be recovered.

ARTICLE INFO

Article history:
Received 10 October 2019
Received in revised form
11 February 2020
Accepted 21 February 2020
Available online 18 March 2020

Keywords:
Syngas recovery
Dry methane reforming
Dual PSA
Simulation

ABSTRACT

In recent years, there has been growing interest in the dry reforming of methane (using CO_2 instead of H_2O) to obtain syngas, due to its economic and environmental advantages. In this reaction, to achieve conversions close to 100%, it is necessary to work at temperatures higher than 1000 °C. However, to attenuate the catalyst deactivation by sintering is convenient to work at lower temperatures, so that normally the syngas (mixture CO + H_2) is obtained mixed with unreacted CO_2 and CH_4. In this work a process has been simulated to recover the syngas from the product of a dry reforming reaction of methane at 700 °C by means of a Dual PSA (Dual Pressure Swing Adsorption) process with heavy reflux using BPL activated carbon as an adsorbent, operating at 25 °C. The process can recover syngas with purity and recovery higher than 99%. Unreacted CO_2 and CH_4 can be recycled to the reactor, leading to effective CO_2 and CH_4 conversions close to 100%. The process specific energy input (SEI) is 4.7 thermal kJ per L (STP) of syngas. The process can also be used to recover the syngas contained in the tail gas of a H_2 purification PSA from SMR-off gas.

Introduction

Interest in dry methane reforming has increased in recent years due to growing concern about global warming and the search for alternative energy sources [1–5]. In the dry reforming of methane, two greenhouse gases, CO_2 and CH_4, are converted into syngas (H_2 and CO, Eq. (1)) which can be used to obtain different chemical products [6–10].

* *Corresponding author.*
E-mail address: jadeldob@ucm.es (J.A. Delgado Dobladez).
https://doi.org/10.1016/j.ijhydene.2020.02.153

$$CO_2 + CH_4 \rightleftharpoons 2\,H_2 + 2\,CO \quad \Delta H^{\circ}_{298K} = 247\ kJ/mol \tag{1}$$

This reaction is endothermic, with a net increase in the number of moles, so it is favored by high temperatures and low pressures [11]. For an operating pressure of 1 bar and a $CO_2/CH_4 = 1$ ratio in the feed, the conversion of methane in equilibrium of this reaction increases with temperature, varying between 90–99% for a temperature range of 800–1000 °C [11].

This reaction is usually carried out in catalytic reactors, using different catalysts such as molybdenum phosphide [12], platinum [13], and nickel [14–19]. Nickel catalysts are most used due to their high reactivity, availability and low cost [20]. These catalysts have the disadvantage that they are deactivated by coke deposition and/or metal sintering. Coke deposition can be reduced by using Ni catalysts with alkaline earth metal oxides and phosphate-zirconia as promoters [20,21]. Metal sintering of Ni catalysts can be reduced by lowering the reaction temperature [22].

Dry methane reforming produces a synthesis gas with a low H_2/CO ratio (theoretically 1:1), which is suitable for the synthesis of oxygenated chemicals [23] and hydrocarbons by means of Fischer-Tropsch synthesis [24]. An interesting application of dry methane reforming is the valorization of biogas through its conversion into syngas. Biogas is a mixture of CO_2 and CH_4 produced by the fermentation of biomass and residues from the agricultural and food industries, which is considered a promising renewable energy source [25]. The transformation of natural gas into syngas has also received much attention as natural gas reserves are larger than oil reserves [26]. The syngas obtained from the dry reforming of methane has also been considered as a form of storage of solar or nuclear energy [27–29].

The production of syngas from dry methane reforming is influenced by the simultaneous occurrence of reverse water gas shift reaction (RWGS) [30], which leads to a H_2/CO ratio lower than 1:

$$CO_2 + H_2 \rightleftharpoons CO + H_2O \quad \Delta H^{\circ}_{298K} = 41\ kJ/mol \tag{2}$$

Although dry methane reforming is very interesting from an economic and environmental point of view, there are still no commercial processes that employ this reaction [31]. Many experimental studies on the dry methane reforming reaction reported in the literature propose to use temperatures near 700 °C at atmospheric pressure [31,32]. This implies that neither CO_2 nor CH_4 is completely converted (as temperatures above 1000 °C are required, as mentioned above), so the reaction product is a mixture of syngas with CO_2 and CH_4, which must be purified to obtain syngas on the one hand, and CO_2 and CH_4 on the other, so that unreacted CO_2 and CH_4 can be recirculated to the reactor. There are few studies in the literature on the recovery of syngas (recovery of CO and H_2 simultaneously) from the dry methane reforming product. Moon et al. [33] have proposed the recovery of syngas (as a mixture of H_2 and CO) from the effluent gas of a melting incinerator ($H_2/CO/CO_2$ mixture) by a PSA process using activated carbon as adsorbent. Most studies on syngas purification in the literature have addressed either the purification of the mixture to obtain H_2, or the removal of CO_2 from the reaction medium [34]. Many studies on syngas purification propose using PSA (pressure swing adsorption) processes, membranes or a combination of both. Chou et al. [35] proposed the simultaneous recovery of concentrated CO_2 and purified H_2 from syngas obtained by reforming methane with steam by PSA. The separation of H_2 from syngas obtained from SMR off-gas by a multi-bed pressure swing adsorption process has been studied by Yang et al. [36]. Li et al. [37] have proposed a pressure swing adsorption/membrane hybrid process. For hydrogen purification with a high recovery. Reddy and Vyas [38] have patented a process for recovering purified H_2 and purified CO_2 from the tail gas of a PSA process for obtaining H_2 from SMR off-gas.

In this work, a process has been designed to recover the syngas of the reaction product of the dry reforming of methane, which consists of a mixture of CO_2, CH_4, CO and H_2. As practically all known adsorbents have a higher selectivity for CO_2 and lower selectivity for H_2 than for the rest of the gases involved, the key factor for selecting an adsorbent for this application is the CH_4/CO selectivity.

BPL activated carbon has been chosen as adsorbent for several reasons: (i) it is a commercial adsorbent that can be used on an industrial scale, (ii) it has a CH_4/CO selectivity higher than other adsorbents studied in the literature (2.87 at 25 °C [39]), such as silicalite (2.71 at 25 °C [40]), and UTSA-16 MOF (2.05 at 25 °C [41]), and (iii) its equilibrium and adsorption kinetics parameters needed to design a PSA process for CO_2–CH_4–CO–H_2 mixtures are known [39,42]. The application of the proposed process to the recovery of syngas from the tail gas of a PSA process for obtaining H_2 from steam methane reforming (SMR) off-gas, which is also a mixture of CO_2, CH_4, CO and H_2, has also been studied [43–45].

Results and discussion

Design of a PSA process for the recovery of syngas from the product of dry reforming of methane

A PSA process using BPL activated carbon as an adsorbent has been designed to recover the syngas produced in a dry methane reforming reactor and recycle the unreacted CO_2 and CH_4 to the reactor to increase the effective conversion of the process. It has been assumed that the gas fed to the PSA from the reactor has the following composition: 42.41% H_2, 45.12% CO, 5.56% CO_2, 6.91% CH_4. This composition has been calculated taking into account the experimental data reported by Alipour et al. [20] on the dry reforming reaction of an equimolar CO_2/CH_4 mixture with a Ni catalyst with MgO as promoter on alumina (5% Ni 3% Mg/Al_2O_3) at 700 °C, in which a CH_4 conversion of 76% is obtained, with an H_2/CO ratio of 0.94 in the product. The formation of coke has been neglected, considering the little deactivation shown by the Ni catalysts promoted with Mg in periods of up to 20 h [20]. For the calculation of the gas composition, it has been considered that the dry reforming reaction occurs in the reactor (Eq. (1)) along with the RWGS reaction (Eq. (2)) [20], and that the water formed by the RWGS reaction is removed before feeding the gas to the PSA process.

Given that the objective of the separation is to obtain a syngas stream (formed by CO and H_2) on the one hand and a CO_2 and CH_4 current on the other, and that the CH_4/CO selectivity of the adsorbent is not very high (2.9), a Dual PSA process has been chosen, as this type of process has a higher separation efficiency than a single PSA process [46]. A Dual PSA process includes two coupled PSA cycles (PSA I and PSA II), where one cycle (PSA I) produces the raffinate enriched in light product, and produces an extract (enriched in the heavy product) that is fed to a second PSA cycle (PSA II). The light product of PSA II is mixed with fresh feed and the mixture is fed to PSA I. The PSA I and PSA II cycles may have different steps. Fig. 1 shows a scheme of a Dual PSA process.

To carry out the separation in each individual PSA process, the cycle proposed by Jiang et al. [47] has been chosen because both light and heavy products with high purity can be obtained. The cycle has been modified by removing an idle step, to increase the cycle productivity. For this purpose, it is necessary to increase the number of beds operating simultaneously in the cycle from three to four. A heavy reflux step has also been included to increase the purity of CO_2 and CH_4 in the heavy product. The same duration is used for almost all the steps because it is usually done so in industrial PSA cycles [48]. The scheme of the PSA cycle is shown in Fig. 2. The step duration times of Dual PSA process are not specified because the Dual PSA cycle includes two PSA cycles working at cyclic steady state, connected by two streams of constant composition, which can be obtained using buffer tanks.

Fig. 1 shows the relationships used to calculate the molar flows of all process streams. The purity of syngas has been calculated as the sum of the molar fractions of H_2 and CO in the light product of PSA I. The purity of the heavy product has been calculated as the sum of the molar fractions of CO_2 and CH_4 in the heavy product of PSA II. The recovery of syngas in the light product has been calculated as:

$$R_{I+II,H2+CO} = \frac{y_{F,H2}(1-R_{I,H2}) + y_{F,CO}(1-R_{I,CO})}{y_{F,H2}(1-R_{I,H2}(1-R_{II,H2})) + y_{F,CO}(1-R_{I,CO}(1-R_{II,CO}))} \quad (3)$$

The productivity of syngas (in moles of syngas in the light product of PSA I per kg of adsorbent in both cycles and per second) is calculated as:

$$P_{I+II,H2+CO} = \frac{y_{F,H2}(1-R_{I,H2}) + y_{F,CO}(1-R_{I,CO})}{\frac{y_{F,H2}(1-R_{I,H2})}{P_{I,H2}} + \frac{y_{F,CO2}\ R_{I,CO2}\ R_{II,CO2}}{P_{II,CO2}}} \quad (4)$$

where $P_{j,i}$ is the productivity of the compound i in PSA j (moles of i in product of cycle j per kg of adsorbent and per s, light product in PSA I and heavy product in PSA II). The energy consumption of the Dual PSA process is (kJ per mole of fresh feed to the process):

$$E_{I+II} = E_I \frac{\sum_{i=1}^{i=n} y_{F,i} R_{I,i}}{\sum_{i=1}^{i=n} y_{F,i}(1-R_{I,i}(1-R_{II,i}))} + E_{II} \frac{\sum_{i=1}^{i=n} y_{F,i} R_{I,i} R_{II,i}}{\sum_{i=1}^{i=n} y_{F,i}(1-R_{I,i}(1-R_{II,i}))} \quad (5)$$

where E_j is the energy consumed by PSA j in kJ per mol of heavy product in PSA j. The energy consumption was calculated assuming isoentropic compression with an efficiency of 60% (Table 1). The fraction between fresh feed and feed of PSA I is calculated as:

$$F_{fresh} \Big/ F = \sum_{i=1}^{i=n} y_{F,i}(1-R_{I,i}(1-R_{II,i})) \quad (6)$$

The PSA processes were simulated with the PSASIM® program. It was assumed that the beds were adiabatic. The equations used to simulate each PSA process are shown in Table 1.

To simulate a PSA cycle, only one bed is simulated undergoing all the cycle steps, since all the beds go through the same sequence of steps. At each step, the molar flow histories coming out of the bed are kept in the computer's memory. These histories are used as boundary conditions (interpolated with Hermite cubic polynomials) in the steps where they are needed. The PDE's system has been discretized with the method of orthogonal collocation in finite elements, with cubic Hermite polynomials, and the resulting ODE system has been solved with the ODEPACK program [49]. Linear pressure

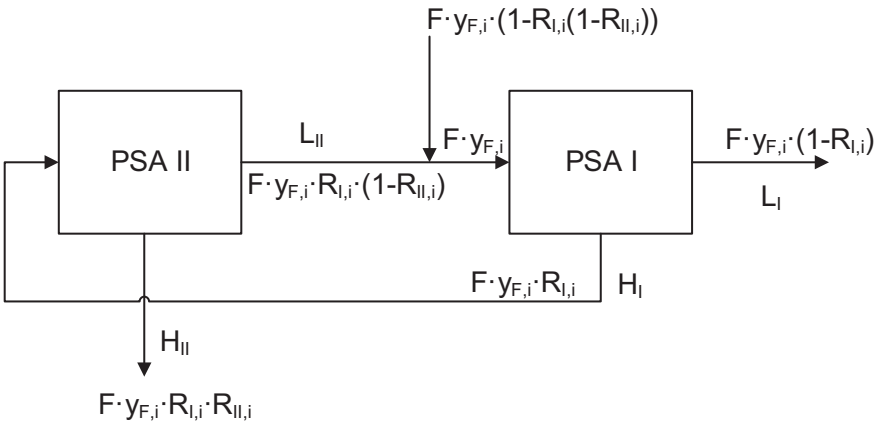

Fig. 1 – Scheme of a dual PSA process. L is the light product and H is the heavy product. F is the number of moles fed to PSA I in one cycle divided into cycle time of PSA I, $y_{F,i}$ is the mole fraction of the i^{th} component in the feed of PSA I, $R_{I,i}$ is the recovery of ith component in the heavy product of PSA I, and $R_{II,i}$ is the recovery of ith component in the heavy product of PSA II.

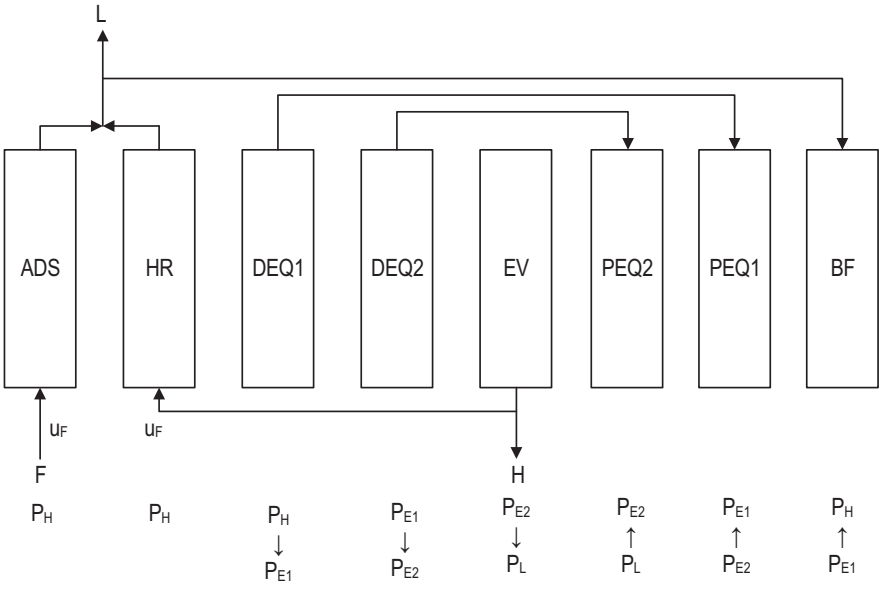

Duration, s	t_{step}	t_{step}	t_{step}	t_{step}	t_{step}	t_{step}	t_{step}	t_{step}
COLUMN 1	ADS	HR	DEQ1	DEQ2	EV	PEQ2	PEQ1	BF
COLUMN 2	PEQ1	BF	ADS	HR	DEQ1	DEQ2	EV	PEQ2
COLUMN 3	EV	PEQ2	PEQ1	BF	ADS	HR	DEQ1	DEQ2
COLUMN 4	DEQ1	DEQ2	EV	PEQ2	PEQ1	BF	ADS	HR

Fig. 2 – Individual PSA cycle in dual PSA configuration for recovering syngas from a $H_2/CO/CH_4/CO_2$ mixture. F = feed gas, L = light product, H = heavy product, P_H = high pressure, P_L = low pressure, P_E = equalization pressure, ADS = feed gas adsorption, HR = heavy reflux, DEQi = ith depressurizing equalization, EV = evacuation, PEQi = ith pressurizing equalization, BF = backfill, u_F = feed gas velocity in the adsorption and heavy reflux step.

variations are assumed in pressure-changing steps (P(t) in Table 1).

To simulate the Dual PSA process, PSA I and PSA II cycles are simulated at the same time, using two executable programs, one for each process. Both programs exchange the information they need to simulate their successive cycles through files that are updated at the end of each cycle. The feed composition of PSA II is obtained from the composition of the heavy product of PSA I (Fig. 1). The feed composition of PSA I is calculated from a mass balance around the mixing node of the fresh feed (Fig. 1), using information from the previous cycle:

$$y_{F,i}\Big|_{cycle\ k+1} = \left[y_{L_{II},i} \sum_{j=1}^{j=n} y_{F,j} R_{I,j}(1-R_{II,j}) + y_{fresh,i} \sum_{j=1}^{j=n} y_{F,j}(1-R_{I,j}(1-R_{II,j})) \right]_{cycle\ k} \quad (7)$$

where the subscript L_{II} refers to L_{II} stream, and the subscript *fresh* refers to the fresh feed to the process. The values of $y_{F,i}$ calculated with Eq. (7) were divided by the sum of $y_{F,i}$ for all components to impose that the sum of $y_{F,i}$ is equal to 1.

Adsorbent properties have been taken from a previous work [39]: particle density = 933 kg m^{-3}, particle porosity = 0.31, particle radius = $4.5 \cdot 10^{-4}$ m, bed porosity = 0.4. The equilibrium parameters (Extended Langmuir equation) of each gas are shown in Table 2.

The kinetic parameters (Table 3) have been obtained by adjusting with the Arrhenius equation the values of reciprocal diffusion time constants reported in the same work (setting $k_s = 15 \times$ reciprocal difusión time constant). For H_2, it has been assumed that $k_s = \infty$ [39].

The adsorption equilibrium and kinetic parameters used have been measured from laboratory experiments in a previous work [39], and they have also been validated with PSA experiments elsewhere [42].

A value of P_L = 0.1 bar has been taken because deep vacuum is economically infeasible and practically difficult at large scale [47]. A low pressure of 0.1 bar is a typical limit considered for practical application of PSA technology [50,51].

The feed gas temperature to both PSA cycles is 25 °C. A parametric study of the effect of the main operating variables (feed velocities, bed length, step duration) on the separation performance has been carried out. The operating conditions and simulation results are shown in Table 4. When analyzing the effect of bed length and feed rate, it was found that the effect of these variables is small if the contact time in the feed step is kept constant (calculated as L/u_F). This can be seen by comparing the results of Runs 1 and 2 (keeping constant L_I/u_{FI}), which are very similar, and the same occurs with the results of Runs 4 and Run 5 (keeping constant L_{II}/u_{FII}). For this reason, the effect of contact time on separation performance has been analysed. Fig. 3 shows the effect of the contact time of PSA I (Runs 7, 3 and 1 in Table 4).

Table 1 – Model for an adiabatic PSA process.

Total mass balance in voids between particles

$$\varepsilon\frac{\partial C}{\partial t} = -\frac{\partial}{\partial z}(u\,C) - (1-\varepsilon)\frac{3}{R_p}\sum_{i=1}^{i=n} k_{macro,i}\,(C\,y_i - c_{macro,i})$$

Mass balance of ith component in voids between particles

$$\varepsilon\frac{\partial(C\,y_i)}{\partial t} = -\frac{\partial}{\partial z}(u\,C\,y_i) + D_L\varepsilon\,\frac{\partial}{\partial z}\left(C\frac{\partial y_i}{\partial z}\right) - (1-\varepsilon)\frac{3}{R_p}k_{macro,i}\,(C\,y_i - c_{macro,i})$$

Mass balance in macropores

$$\varepsilon_p\frac{\partial c_{macro,i}}{\partial t} = \frac{3}{R_p}k_{macro,i}\,(C\,y_i - c_{macro,i}) - \rho_p\,k_{s,i}\,(n_i^*(c_{macro}) - n_i)$$

Mass balance in micropores

$$\frac{\partial n_i}{\partial t} = k_{s,i}\,(n_i^*(c_{macro}) - n_i)$$

Equation of state Momentum balance

$$C = \frac{P}{R\,T_g} \qquad -\frac{\partial P}{\partial z} = \frac{150\,\mu(1-\varepsilon)^2}{\varepsilon^3 4\,R_p^2}u + \frac{1.75\,(1-\varepsilon)\rho_g}{\varepsilon^3 2\,R_p}u^2$$

Multicomponent adsorption isotherm (Extended Langmuir)

$$n_i = \frac{n_{max,i}\,b_i\,p_i}{1+\sum_{j=1}^{j=n} b_j\,p_j} \qquad b_i = b_{0,i}\,exp\left(\frac{-\Delta H_i}{RT}\right)$$

Energy balance in the gas phase (adiabatic column) Solid-gas heat transfer correlation

$$\frac{\partial}{\partial t}(\varepsilon\,c_{vg}CT_g) = \lambda\frac{\partial^2 T}{\partial z^2} - \frac{\partial}{\partial z}(u\,C\,c_{pg}T_g) + (1-\varepsilon)\frac{3}{R_p}h_{sg}(T_s - T_g) \quad h_{sg} = \frac{k_g}{2\,R_p}(2+1.1\;Re^{0.6}Pr^{1/3})$$

Energy balance in the adsorbent

$$\frac{\partial}{\partial t}(\rho_p c_{ps}T_s + \varepsilon_p c_{vg}T_s\sum_{i=1}^{i=n} c_{macro,i}) = \rho_p\sum_{i=1}^{i=n}\left((-\Delta H_i)\frac{\partial n_i}{\partial t}\right) - \frac{3}{R_p}h_{sg}(T_s - T_g)$$

Gas-solid mass transfer correlation Gas-macropore mass transfer coefficient

$$k_f = \frac{u}{\varepsilon\,Sc^{2/3}}\left(\frac{0.765}{Re^{0.82}} + \frac{0.365}{Re^{0.386}}\right) \qquad k_{macro} = \left(\frac{1}{\frac{5D_m\varepsilon_p}{\tau\,R_p}} + \frac{1}{k_f}\right)^{-1}$$

Axial dispersion correlations Mass transfer coefficient in micropores

$$D_L = 0.73\,D_m + \frac{u\,R_p/\varepsilon}{1+\frac{9.49\,\varepsilon\,D_m}{2\,u\,R_p}} \qquad \lambda = k_g(10+0.5\,Re\,Pr) \qquad k_{s,i} = k_{s0,i}\,exp\left(-\frac{E_{diff,i}}{RT}\right)$$

Compression energy

$$Energy\ per\ cycle\ (J) = \int_0^{t_{evacuation}} (mole\ flow\ rate\ out)\frac{kRT_{g,out}}{(k-1)\eta_C}\left[\left(\frac{P_{atm}}{P_{out}}\right)^{\frac{k-1}{k}} - 1\right]dt \quad k = \frac{c_{pg}}{c_{vg}} \quad \eta_C = 0.6$$

Boundary conditions for steps with specified outlet pressure (e.g. adsorption)

Boundary conditions for total mass balance

$$z = z_{inlet}\;u\,C = molar\ flux\ in \qquad z = z_{outlet}\;P = outlet\ pressure$$

Boundary conditions for mass balance of ith component

$$z = z_{inlet}\;u\,C\,y_i - \varepsilon\,D_L C\frac{\partial y_i}{\partial z} = molar\ flux\ of\ i^{th}\ component\ in \quad z = z_{outlet}\frac{\partial y_i}{\partial z} = 0$$

Boundary conditions for energy balance

$$z = z_{inlet} \quad u\,C\,c_{pg}\,T_g - \lambda\frac{\partial T_g}{\partial z} = (molar\ flux\ in)\,c_{pg}\,T_{inlet} \qquad z = z_{outlet}\frac{\partial T_g}{\partial z} = 0$$

Boundary conditions for pressure-changing steps (e.g. pressurization)

Boundary conditions for total mass balance

$$z = z_{with\ pressure\ variation}\;P = P(t) \quad z = z_{closed}\frac{\partial P}{\partial z} = 0$$

Boundary conditions for mass balance of ith component

$$z = z_{with\ pressure\ variation}\;u(y_i - y_{i,in}) - \varepsilon\,D_L\frac{\partial y_i}{\partial z} = 0 \quad z = z_{closed}\frac{\partial y_i}{\partial z} = 0$$

Boundary conditions for energy balance

$$z = z_{with\ pressure\ variation}\;u\,C\,c_{pg}\,(T_g - T_{g,in}) - \lambda\,\frac{\partial T_g}{\partial z} = 0 \quad z = z_{closed}\frac{\partial T_g}{\partial z} = 0$$

Boundary conditions for steps with specified molar inlet flux (e.g. pressurizing equalization)

Boundary conditions for total mass balance

$$z = z_{inlet}\;u\,C = molar\ flux\ in \quad z = z_{closed}\frac{\partial P}{\partial z} = 0$$

Boundary conditions for mass balance of ith component

$$z = z_{inlet}\;u\,C\,y_i - \varepsilon\,D_L C\frac{\partial y_i}{\partial z} = \text{molar flux of i}^{th}\text{ component in} \quad z = z_{closed}\frac{\partial y_i}{\partial z} = 0$$

Boundary conditions for energy balance

$$z = z_{inlet}\;u\,C\,c_{pg}\,T_g - \lambda\frac{\partial T_g}{\partial z} = (molar\ flux\ in)\,c_{pg}\,T_{inlet} \quad z = z_{closed}\frac{\partial y_i}{\partial z} = 0$$

Initial conditions

$$P = P_{initial}\;y_i = y_{i,initial}\;T_g = T_{initial}\;T_s = T_{initial} \quad n_i = n_{i,initial}\text{ at equilibrium with P }y_{i,initial}\text{ at }T_{initial}$$

Table 2 – Langmuir parameters of H_2/CO/CO_2/CH_4 on BPL activated carbon.

Parameter	H_2	CH_4	CO	CO_2
n_{max} (mol kg^{-1})	1.790	2.731	1.818	4.25
b_0 (Pa^{-1})	$1.33 \cdot 10^{-8}$	$1.61 \cdot 10^{-9}$	$1.59 \cdot 10^{-9}$	$3.93 \cdot 10^{-10}$
-ΔH (kJ mol^{-1})	5.93	20.27	18.69	25.04

It is observed that the purity of the syngas increases as the contact time increases. This is because the longer the contact time the strong adsorbates have more time to be adsorbed as they pass through the bed in the adsorption step, thus lowering their concentration in the outlet stream (light product). This can be seen in Fig. 4, where the mole fraction profiles in the bed at the end of the adsorption step in PSA I are compared for the cases with $L_I/u_{FI} = 7$ and 12 s. For a contact time of 7s, methane concentration front reaches the end of the bed, which lowers the purity of the syngas obtained (94.76%, Run 7 in Table 4), while with a time of 12 s the concentration fronts of CO_2 and CH_4 do not reach the end of the bed, so the purity of the syngas obtained is very high (+99.99%, Table 4). Productivity decreases as L_I/u_{FI} increases (Fig. 3) because the bed adsorption capacity is less used. The decrease in productivity results in an increase of the energy consumed (Fig. 3).

It is observed that when L_{II}/u_{FII} goes up, the purity of the syngas increases and the recovery decreases. This is because raising this variable reduces the amount of CO_2 and CH_4 in the light product of PSA II, and therefore a smaller amount of these components reaches PSA I (Fig. 1). This can be seen in Fig. 6, which shows the effect of L_{II}/u_{FII} on the mole fraction profiles in the gas at the end of the adsorption step in PSA II.

The productivity of syngas decreases when L_{II}/u_{FII} increases because CO recovery decreases. This is seen in Fig. 7, where the effect of L_{II}/u_{FII} on the concentration profiles at the end of the adsorption step in PSA I is shown. As the L_{II}/u_{FII} rises, the bed is loaded with less CO_2 and CH_4, which causes more CO to be lost in the heavy product. The energy consumed per mol of fresh feed decreases when rising L_{II}/u_{FII} because the flowrate of fresh feed rises (F_{fresh}/F increases, Runs 5 and 6 in Table 4).

It is observed that as the t_{step} rises the purity of the syngas decreases and the recovery of syngas increases. As t_{step} rises, more gas is fed and the CO_2 and CH_4 concentration fronts advance more through the bed, especially the CH_4 (heavy key component) so the light product is impurified with CH_4. Syngas recovery increases because the heavy product of PSA I contains less syngas, as the bed is loaded with more CO_2 and CH_4 prior to evacuation. Productivity increases and energy decreases as t_{step} increases because the adsorption capacity of the bed is used to a greater extent.

Table 3 – Mass transfer parameters in micropores of BPL activated carbon (for Arrhenius equation in Table 1).

Parameter	CH_4	CO	CO_2
k_{s0} (s^{-1})	1960	577	7918
E_{diff} (kJ mol^{-1})	17.7	11.3	23.6

Table 4 – Operating conditions and separation performance results for different feed gas compositions.

Run	L_I, m	L_{II}, m	t_{step}, s	t_{HR}, s	$u_{F,I}$, m/s	$u_{F,II}$, m/s	$L_I/u_{F,I}$, s	$L_{II}/u_{F,II}$, s	Pur_{H2+CO}, %	Rec_{H2+CO}, %	$Prod_{H2+CO}$, mol kg^{-1} s^{-1}	$Pur_{CO2+CH4}$, %	F_{fresh}/F	$y_{F,H2}$	$y_{F,CO}$	$y_{F,CO2}$	E_{I+II}, kJ/mol_{fresh}
[a]1	1	0.3	20	0	0.083	0.6	12	0.5	+99.99	98.98	$4.81 \cdot 10^{-4}$	93.31	0.28	0.1187	0.3393	0.1794	30.67
[a]2	1.236	0.3	20	0	0.103	0.6	12	0.5	+99.99	98.96	$4.80 \cdot 10^{-4}$	93.22	0.28	0.1185	0.3411	0.1790	31.34
[a]3	1	0.3	20	0	0.103	0.6	9.71	0.5	99.75	99.80	$4.87 \cdot 10^{-4}$	98.58	0.31	0.1322	0.2056	0.2162	27.02
[a]4	1	0.3	20	0	0.103	0.429	9.71	0.7	99.93	99.33	$4.83 \cdot 10^{-4}$	95.49	0.37	0.1570	0.3137	0.1741	21.36
[a]5	1	0.42	20	0	0.103	0.6	9.71	0.7	99.93	99.31	$4.83 \cdot 10^{-4}$	95.35	0.37	0.1579	0.3170	0.1720	21.33
[a]6	1	0.3	20	0	0.103	1	9.71	0.3	96.79	99.94	$4.93 \cdot 10^{-4}$	99.41	0.27	0.1134	0.1563	0.3165	32.41
[a]7	1	0.3	20	0	0.143	0.6	7	0.5	94.76	99.85	$4.95 \cdot 10^{-4}$	98.33	0.44	0.1879	0.2797	0.3031	15.63
[a]8	1	0.3	15	0	0.103	0.6	9.71	0.5	+99.99	97.28	$4.48 \cdot 10^{-4}$	83.95	0.30	0.1261	0.4713	0.1385	29.34
[a]9	1	0.3	25	0	0.103	0.6	9.71	0.5	95.23	99.91	$5.83 \cdot 10^{-4}$	99.06	0.37	0.1575	0.2216	0.3320	19.7
10	1	0.3	20	1	0.103	0.6	9.71	0.5	96.05	99.99	$4.22 \cdot 10^{-4}$	99.87	0.28	0.1173	0.1582	0.3073	32.5
11	1	0.3	20	2	0.103	0.6	9.71	0.5	92.97	99.99	$3.20 \cdot 10^{-4}$	99.99	0.22	0.0914	0.1067	0.6448	46.5
12	1	1	20	5	0.115	0.41	8.70	2.44	99.77	99.84	$8.07 \cdot 10^{-4}$	98.86	0.58	0.2455	0.4531	0.0889	14.8
13	1	1	20	10	0.115	0.235	8.70	4.36	99.89	99.91	$8.22 \cdot 10^{-4}$	99.38	0.71	0.3030	0.4985	0.0566	14.0
14	1	1	20	20	0.128	0.0843	7.81	11.9	99.83	99.95	$7.85 \cdot 10^{-4}$	99.65	0.96	0.4081	0.4718	0.0535	16.3
[b]15	1	1	20	0	0.103	0.4	9.71	2.5	99.63	99.61	$2.76 \cdot 10^{-4}$	99.70	0.44	0.1407	0.0707	0.6012	26.89

[a] Feed gas = 42.41% H_2, 45.12% CO, 5.56% CO_2, 6.91% CH_4.
[b] Feed gas = 32.20% H_2, 11.30% CO, 48.02% CO_2, 8.48% CH_4.

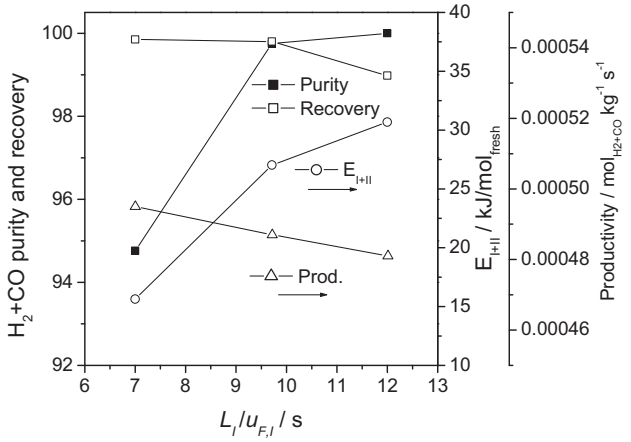

Fig. 3 – Effect of L_I/u_{FI} on separation performance.

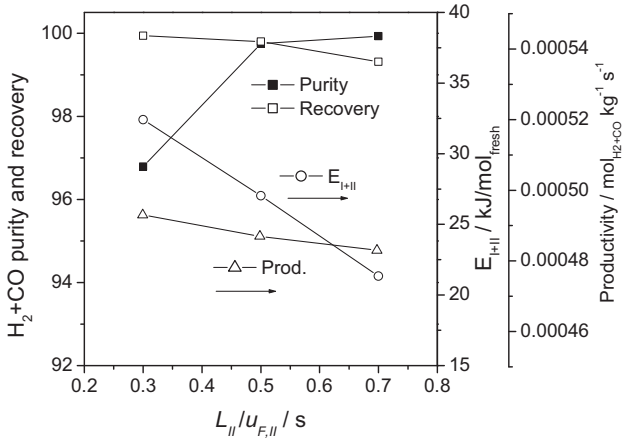

Fig. 5 – Effect of L_{II}/u_{FII} on separation performance.

The effect of increasing the amount of gas introduced into the heavy reflux step (increasing the duration of the heavy reflux step, t_{HR}) can be seen in Table 4 with Runs 3, 10 and 11. Increasing t_{HR} results in an increase of the purity of heavy product and the recovery of syngas in the light product. This suggests that, if t_{HR} is increased, the contact time in PSA II can be increased to reach the same purity of the heavy product, thereby reducing energy consumption (see Runs 3 and 5 in Table 4). In addition, it is also seen that if the contact time of PSA II is increased, the purity of the syngas increases (Fig. 5), so that the contact time of PSA I can be lowered to reach the same purity of the light product.

Bearing this in mind, the process has been designed with different values of duration of the HR step, looking for purity and recovery of syngas in the light product above 99% (Runs 12, 13 and 14 in Table 4). A recovery value above 99% for a PSA process has been proposed by Kuah et al. [52]. To this end, the contact times of PSA I and PSA II have been changed to achieve this objective. It is observed that there is an optimum proportion of gas volumes in the ADS/HR steps with which minimum energy consumption (14 kJ $mol^{-1}_{fresh\ feed}$) and maximum productivity ($8.22 \cdot 10^{-4}$ mol kg^{-1} s^{-1}) are achieved, with purity and syngas recovery above 99% (Run 13 in Table 4). Although according to engineering experience for operation with single PSA units it is difficult to achieve recoveries above 95%, simulation results with a model based in conservation equations show that it is possible to achieve recoveries above 99% with a Dual PSA process.

Fig. 9 shows a flow diagram of the Dual PSA process with operating conditions of Run 13 in Table 4.

All H_2 in the feed is recovered in PSA I. Part of the CO in the feed passes from PSA I to PSA II, but is recovered in the light product of PSA II, so that very little is lost in the heavy product of PSA II. The concentration of CO_2 and CH_4 rises progressively

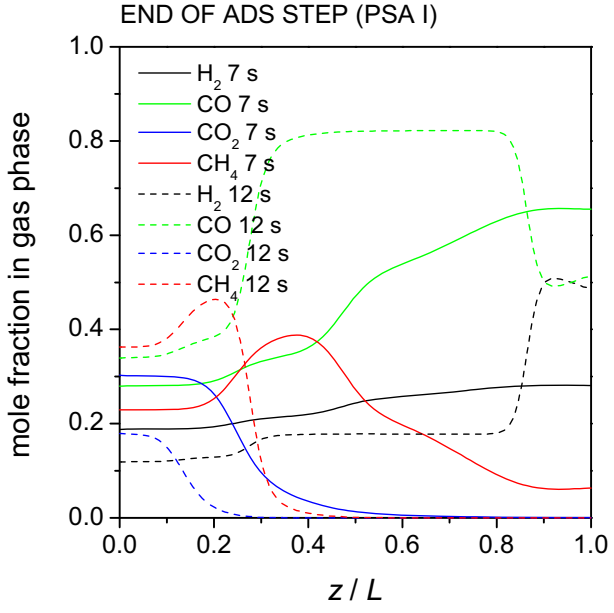

Fig. 4 – Effect of L_I/u_{FI} (in s) on mole fraction profiles. The effect of L_{II}/u_{FII} on separation is shown in Fig. 5 (Runs 6, 3 and 5 in Table 4).

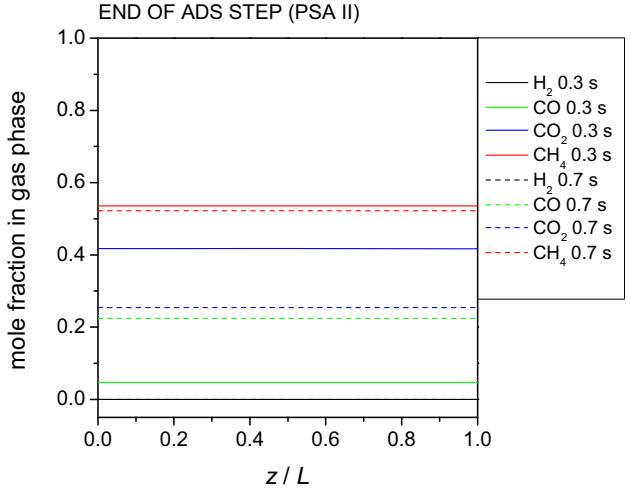

Fig. 6 – Effect of L_{II}/u_{FII} (in s) on mole fraction profiles of PSA II.

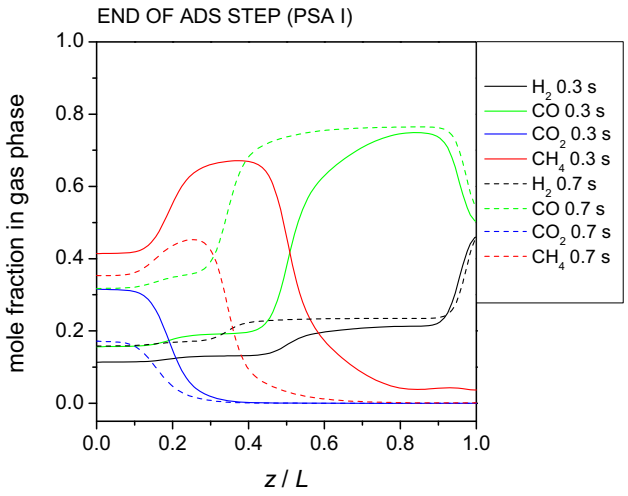

Fig. 7 – Effect of L_{II}/u_{FII} (in s) on mole fraction profiles of PSA I. The effect of the step duration (t_{step}) on the separation is shown in Fig. 8 (Runs 8, 3 and 9 in Table 4).

from fresh feed to feed of PSA I (by mixing with L_{II}), then grows in the heavy product of PSA I, to finally reach the maximum value in the heavy product of PSA II. Fig. 10 shows the initial and final profiles in the evacuation step (EV) of PSA II. The heavy end of the bed is mainly loaded with CO_2 and CH_4 during evacuation, which explains the low concentration of CO and H_2 in the heavy PSA II product. Fig. 11 shows the initial profiles in the ADS step and the final ones in the HR stage. The purity of syngas is high because during the ADS and HR stages the CO_2 and CH_4 concentration fronts do not reach the light end of the bed.

The energy consumption of the process producing syngas by dry methane reforming at 700 °C integrated with the recovery of syngas by Dual PSA has been calculated using the AspenPlus® program. Fig. 12 shows a flow diagram of the process considered for the calculation of energy consumption. To calculate the energy consumption in the reactor, the energy consumption due to the pressure drop has been

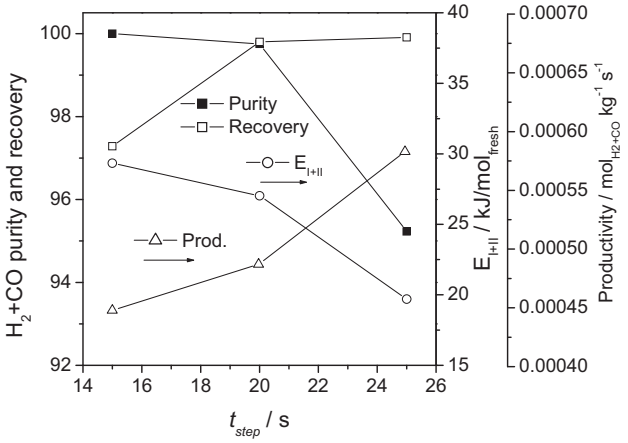

Fig. 8 – Effect of t_{step} on separation performance.

neglected, as it is very small compared to the heat input [11]. Energy consumption due to pressure drop through heat exchangers has also been neglected [52]. To calculate the energy consumption of the Dual PSA process, only the consumption due to gas compression has been considered [52,53]. A heater connected to the reactor is used to reach the reaction temperature, which operates at 700 °C and 1 bar. The reactor was simulated with the RSTOIC module. The reactor consumes energy because the reactions that occur are endothermic. The product is cooled to 35 °C to recover heat, and then cooled to 25 °C to be sent to a drying process where the water produced by the RWGS reaction (Eq. (2)). Drying has been considered to consume 8 MJ per kg of water withdrawn [54]. The resulting stream is sent to the Dual PSA, where the syngas is obtained and the unreacted CO_2+CH_4 mixture is recycled to the reactor. Due to the RWGS reaction, the CO_2 conversion is greater than the CH_4 conversion, so it is necessary to add additional CO_2 to maintain an equimolar CO_2/CH_4 ratio at the reactor inlet. To simulate the Dual PSA in Aspenplus®, a SEP2 module has been used assuming that the concentrations of CO_2 and CH_4 in the light product, and those of H_2 and CO in the heavy product, are the same as in the Run 13 in Table 4. The thermal energy consumption of the Dual PSA has been calculated considering that each unit of (electrical) compression energy corresponds to 2.5 units of thermal energy. The calculation has been carried out as follows:

Thermal energy consumption (kJ/mol syngas) = (44.9 + 130.5 − 50.4 + 0.0308*18*8 + 2.277*14.0*2.5)/1.994 = 104.9.

Specific energy input (SEI, kJ/L (STP)) = 104.9/22.4 = 4.7.

This energy consumption has been compared with that reported for other alternatives to carry out the syngas production process through dry methane reforming with conversions close to 100%. The value obtained with the proposed process is less than that required with a plasma reactor (11.2 kJ (electrical)/L [55]). Luyben [11] has designed a process to obtain syngas by methane dry reforming using a fired reactor with Ni catalyst operating at 1000 °C and 4 bar. The thermal energy consumption required to obtain syngas at 1.5 bar and 50 °C is 72 kJ/mol syngas (SEI 3.2 kJ/L). Although the energy consumption of the proposed process is greater than this value, it must be considered that this process involves working at 1000 °C instead of 700 °C in the reactor, which implies greater deactivation of the catalyst by sintering [22,56], consumption of heat with higher quality (the source of heat is at higher temperature), and the need for more expensive materials to build the reactor.

The calculation of bed size and the economic calculation of adsorbent cost for an equimolar CO_2/CH_4 feed stream of 1000 kmol h^{-1} is available in Appendix A(Supplementary Material). The bed size required using four Dual PSA units is 9 m of diameter and 1 m of length, which is comparable to the bed size of other industrial adsorption processes [57]. The adsorbent cost assuming an adsorbent lifetime of 10 years [58] and an adsorbent price of 800 USdollar per ton [59] is 0.14 USDollar per TCM (thousand cubic meter) of syngas. This cost is acceptable considering that the production cost of syngas from natural gas is 24–90 USdollar per TCM [60].

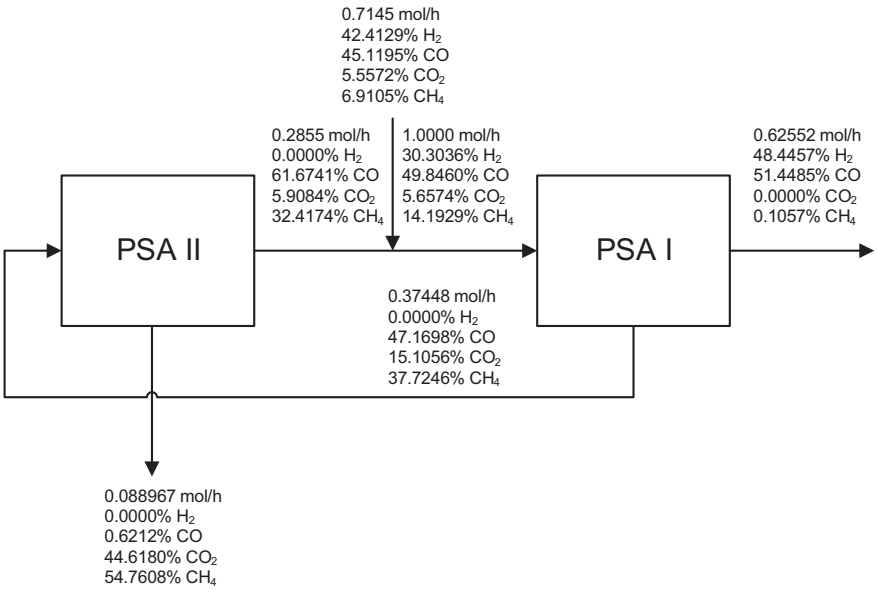

Fig. 9 – Flowsheet of the Dual PSA process with operating conditions of Run 13 in Table 4.

Recovery of syngas from the tail gas of a PSA for H_2 purification from SMR off-gas

Another possible application of the proposed Dual PSA process is the recovery of syngas from the tail gas of a PSA process for obtaining hydrogen from steam methane reforming (SMR). In these processes, high purity hydrogen (>99.99) is obtained from a mixture containing H_2, CO, CO_2 and CH_4 [43–45], and a waste gas is produced containing the unrecovered H_2, and virtually all the CO, CO_2 and CH_4 in the feed. Normally this gas is sent to an oven to obtain energy [45], but it can be used more efficiently if H_2 and CO (syngas) are separated from CO_2 and CH_4 (raw material for the dry reforming of methane), as two valuable products are obtained. A Dual PSA process has been designed to recover syngas from a waste gas from a typical PSA process for obtaining H_2 from SMR. To calculate the composition of the waste gas, a typical composition of the gas fed to the PSA producing H_2 has been assumed (76% H_2, 4% CO, 17% CO_2, 3% CH_4), and it has been assumed that the PSA process achieves an 85% H_2 recovery [44,45]. Thus, the tail gas has a composition of 32.20% H_2, 11.30% CO, 48.02% CO_2 and 8.48% CH_4. The same high- and low-pressure values of the cycles have been maintained. Operating conditions and separation performance are shown in Table 4 (Run 15). The flow diagram of the Dual PSA process designed is shown in Fig. 13. It is also possible to recover syngas efficiently from this waste gas with the proposed process, with purity and recovery above 99%. This indicates that this process has a good capacity to adapt to changes in the composition of the feed gas. The H_2/CO ratio of the syngas obtained is higher than in the previous case due to the lower proportion of CO in the feed gas. In this case it has not been necessary to include the HR stage, due to the higher CO_2 content of the gas to be treated (48 vs. 5.6%), so that a high concentration of CO_2 in the heavy product can be achieved without the need for the HR step.

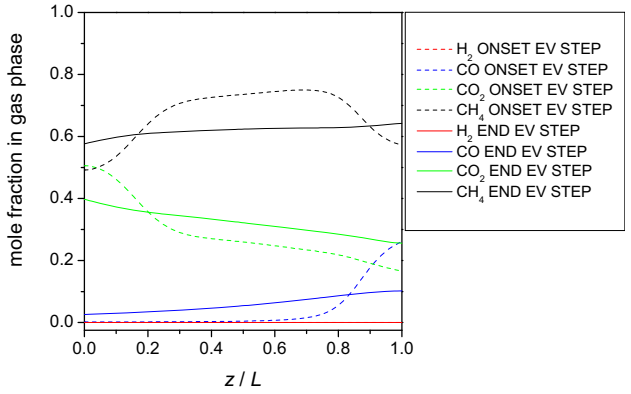

Fig. 10 – Mole fraction profiles in EV step of PSA II in Run 13 in Table 4.

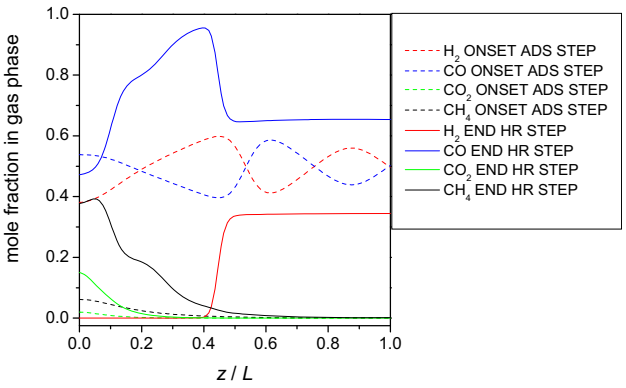

Fig. 11 – Mole fraction profiles in ADS and HR steps of PSA I in Run 13 in Table 4.

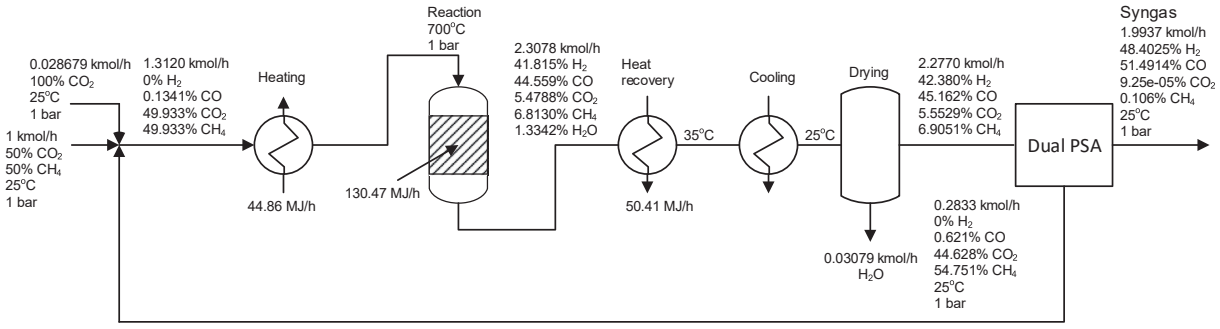

Fig. 12 – Flowsheet of the methane dry reforming process at 700 °C integrated with syngas recovery by Dual PSA.

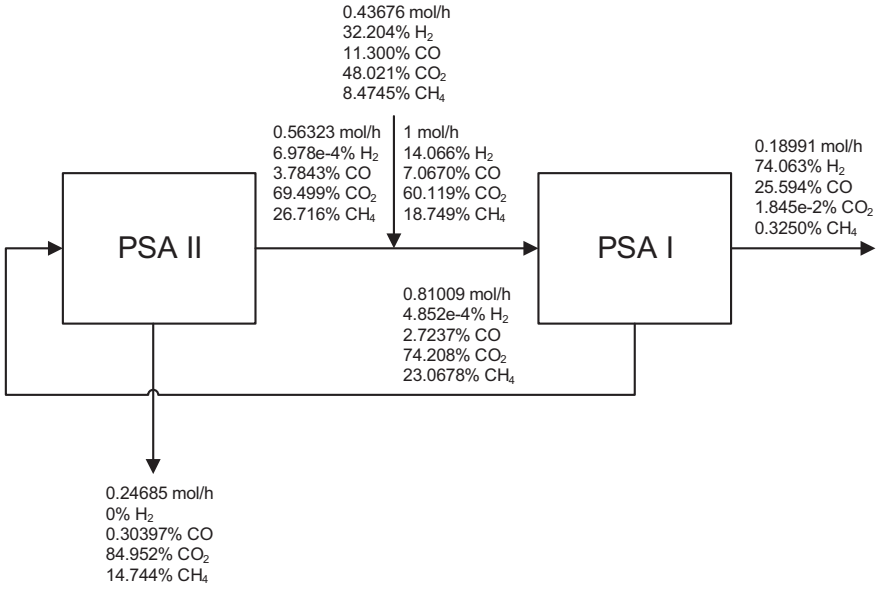

Fig. 13 – Flowsheet of the Dual PSA process with operating conditions in Run 15 in Table 4.

Conclusions

A Dual PSA process has been designed to recover syngas from a dry methane reforming process using BPL activated carbon as adsorbent operating at 25 °C. The process can recover syngas with purity and recovery greater than 99% of a reaction product obtained with a Ni catalyst with MgO promoter at 700 °C, so that the effective conversion of the reactor can be raised to almost 100%. The energy consumption of the process (SEI = 4.7 kJ/L thermal) is notably lower than that reported for plasma reactors, and higher than that reported for a Ni catalytic reactor operating at 1000 °C, but with the advantage of operating at 700 °C instead of 1000 °C. The proposed Dual PSA process can be used for the efficient recovery of syngas and CO_2/CH_4 mixture from the waste gas of a PSA producing H_2 from SMR off-gas.

Acknowledgement

Financial support from the Ministry of Economy and Competitiveness of Spain through project CTM2017-84033-R is gratefully acknowledged.

Appendix A. Supplementary data

Supplementary data to this article can be found online at https://doi.org/10.1016/j.ijhydene.2020.02.153.

Notation

$b_{0,i}$	preexponential constant of b_i, Pa^{-1}
b_i	adsorption affinity of ith component, Pa^{-1}
C	total concentration, mol m^{-3}
$c_{macro,i}$	concentration of ith component in macropores, mol m^{-3}
c_{pg}	gas heat capacity at constant pressure, J mol^{-1} K^{-1}
c_{ps}	heat capacity of solid adsorbent, J kg^{-1} K^{-1}
c_{vg}	gas heat capacity at constant volume, J mol^{-1} K^{-1}
D_L	axial dispersion coefficient, m^2 s^{-1}
D_m	molecular diffusivity, m^2 s^{-1}
$E_{diff,i}$	activation energy of diffusion of ith component, J mol^{-1}
E_I	Compression energy consumption in PSA I, kJ per mol of fresh feed

h_{sg}	heat transfer coefficient between gas and solid, J m^{-2} s^{-1} K^{-1}
k	c_{pg}/c_{vg} ratio
k_f	external mass transfer coefficient, m s^{-1}
k_g	gas heat conductivity, J m^{-1} s^{-1} K^{-1}
$k_{macro,i}$	mass transfer coefficient between gas and macropores of ith component, m s^{-1}
$k_{s,i}$	mass transfer coefficient of ith component between macropores and micropores, s^{-1}
$k_{s0,i}$	preexponential constant of $k_{s,i}$, s^{-1}
L	bed length, m
n_i	adsorbed concentration of ith component, mol kg^{-1}
p	partial pressure, Pa
P	total pressure, Pa
$P_{I,i}$	productivity of ith component in light product of PSA I, mol kg^{-1} s^{-1}
Pr	Prandtl number, c_{pg} μ/k_g
R	gas constant, 8.31 J mol^{-1} K^{-1}
Re	Reynolds number, ρ u 2 R_p/μ
$R_{I,i}$	recovery of ith component in PSA I
R_p	particle radius, m
Sc	Schmidt number, μ ρ/D_m
t	time, s
T_g	gas temperature, K
T_s	solid adsorbent temperature, K
t_{step}	step duration, s
u	superficial velocity, m s^{-1}
y	mole fraction
z	axial coordinate, m
ΔH	adsorption enthalpy, J mol^{-1}

Greek letters

ε	bed porosity
ε_p	particle porosity
λ	heat axial dispersion coefficient, J m^{-1} s^{-1} K^{-1}
μ	gas viscosity, Pa s
ρ_p	particle density, kg m^{-3}
ρ_g	gas density, kg m^{-3}
τ	tortuosity
η_C	isentropic compression efficiency

REFERENCES

[1] Seo HO. Recent scientific progress on developing supported Ni catalysts for dry (CO_2) reforming of methane. Catalysts 2018;8:110. https://doi.org/10.3390/catal8030110.

[2] Sheng Z, Kameshima S, Sakata K, Nozaki T. Plasma-enabled dry methane reforming. In: Britun N, Silva T, editors. Plasma chemistry and gas conversion. Intechopen; 2018. DOI: 110.5772/intechopen.80523.

[3] Liao CH, Horng RF. Experimental study of syngas production from methane dry reforming with heat recovery strategy. Int J Hydrogen Energy 2017;42:25213–24.

[4] Varsano F, Bellusci M, La Barbera A, Petrecca M, Albino M, Sangregorio C. Dry reforming of methane powered by magnetic induction. Int J Hydrogen Energy 2019;44:21037–44.

[5] Ren J, Li M, Lee AC, Cheng K, Chen Y. IR spectroscopic measurement of hydrogen production kinetics in methane dry reforming. Int J Hydrogen Energy 2019;44:9866–72.

[6] Lebouvier A, Iwarere SA, d'Argenlieu P, Ramjugernath D, Fulcheri L. Assessment of carbon dioxide dissociation as a new route for syngas production: a comparative review and potential of plasma based technologies. Energy Fuels 2013;27:2712–22.

[7] Lieuwen TC, Yang V, Yetter R, editors. Synthesis gas combustion: fundamentals and applications. Boca Raton: CRC Press; 2009.

[8] Wilhelm DJ, Simbeck DR, Karp AD, Dickenson RL. Syngas production for gas-to-liquids applications: technologies, issues and outlook. Fuel Process Technol 2001;71:139–48.

[9] Hunt AJ, Sin EHK, Marriott R, Clark JH. Generation, capture, and utilization of industrial carbon dioxide. ChemSusChem 2010;3:306–22.

[10] Martens JA, Bogaerts A, De Kimpe N, Jacobs PA, Marin GB, Rabaey K, Saeys M, Verhelst S. The chemical route to a carbon dioxide neutral world. ChemSusChem 2017;10:1039–55.

[11] Luyben WL. Design and control of the dry methane reforming process. Ind Eng Chem Res 2014;53:14423–39.

[12] Cui Y, Liu Q, Yao Z, Dou B, Shi Y, Sun Y. A comparative study of molybdenum phosphide catalyst for partial oxidation and dry reforming of methane. Int J Hydrogen Energy 2019;44:11441–7.

[13] da Fonseca RO, Rabelo-Neto RC, Simoes RCC, Mattos LV, Noronha FB. Pt supported on doped CeO_2/Al_2O_3 as catalyst for dry reforming of methane. Int J Hydrogen Energy 2019;45:5182–91. https://doi.org/10.1016/j.ijhydene.2019.09.207.

[14] Rego de Vasconcelos B, Minh DP, Martins E, Germeau A, Sharrock P, Nzihou A. Highly-efficient hydroxyapatite-supported nickel catalysts for dry reforming of methane. Int J Hydrogen Energy 2020;45:18502–18. https://doi.org/10.1016/j.ijhydene.2019.08.068.

[15] Aguiar M, Cazula BB, Colpini LMS, Borba CE. Si-MCM-41 obtained from different sources of silica and its application as support for nickel catalysts used in dry reforming of methane. Int J Hydrogen Energy 2019;44:32003–18.

[16] Barelli L, Bidini G, Di Michele A, Gammaitoni L, Mattarelli M, Mondi F, Sisani E. Development and validation of a Ni-based catalyst for carbon dioxide dry reforming of methane process coupled to solid oxide fuel cells. Int J Hydrogen Energy 2019;44:16582–93.

[17] Shen J, Reule AAC, Semagina N. Ni/MgAl2O4 catalyst for low-temperature oxidative dry methane reforming with CO_2. Int J Hydrogen Energy 2019;44:4616–29.

[18] Kumar N, Kanitkar S, Wang Z, Haynes D, Shekhawat D, Spivey JJ. Dry reforming of methane with isotopic gas mixture over Ni-based pyrochlore catalyst. Int J Hydrogen Energy 2019;44:4167–76.

[19] Leba A, Yildirim R. Determining most effective structural form of nickel-cobalt catalysts for dry reforming of methane. Int J Hydrogen Energy 2019;45:4268–83. https://doi.org/10.1016/j.ijhydene.2019.12.020.

[20] Alipour Z, Rezaei M, Meshkani F. Effect of alkaline earth promoters (MgO, CaO, and BaO) on the activity and coke formation of Ni catalysts supported on nanocrystalline Al_2O_3 in dry reforming of methane. J Ind Eng Chem 2014;20:2858–63.

[21] Ibrahim AA, Al-Fatesh AS, Khan WU, Kasim SO, Abasaeed AE, Fakeeha AH, Bonura G, Frusteri F. Enhanced coke suppression by using phosphate-zirconia supported nickel catalysts under dry methane reforming conditions. Int J Hydrogen Energy 2019;44:27784–94.

[22] Bartholomew CH, Sorensen WL. Sintering kinetics of silica- and alumina-supported nickel in hydrogen atmosphere. J Catal 1983;81:131–41.

[23] Wurzel T, Malcus S, Mleczko L. Reaction engineering investigations of CO_2 reforming in a fluidized-bed reactor. Chem Eng Sci 2000;5:3955–66.

[24] Oyama ST, Hacarlioglu P, Gu Y, Lee D. Dry reforming of methane has no future for hydrogen production: comparison with steam reforming at high pressure in standard and membrane reactors. Int J Hydrogen Energy 2012;37:10444–50.
[25] Goula G, Kiousis V, Nalbandian L, Yentekakis IV. Catalytic and electrocatalytic behavior of Ni-based cermet anodes under internal dry reforming of CH_4+CO_2 mixtures in SOFCs. Solid State Ionics 2006;177:2119–23.
[26] Song X, Guo Z. Technologies for direct production of flexible H_2/CO synthesis gas. Energy Convers Manag 2006;47:560–9.
[27] Levy M, Levitan R, Meirovitch E, Segal A, Rosin H, Rubin R. Chemical reactions in a solar furnace 2: direct heating of a vertical reactor in an insulated receiver. Experiments and computer simulations. Sol Energy 1992;48:395–402.
[28] Chubb TA. Characteristics of CO_2/CH_4 reforming-methanation cycle relevant to the solchem thermochemical power system. Sol Energy 1980;24:341–5.
[29] Fraenkel D, Levitan R, Levy M. A solar thermochemical pipe based on the CO_2/CH_4 (1:1) system. Int J Hydrogen Energy 1986;11:267–77.
[30] Bradford MCJ, Vannice MA. CO_2 reforming of CH_4. Catal Rev 1999;41:1–42.
[31] Arora S, Prasad R. An overview on dry reforming of methane: strategies to reduce carbonaceous deactivation of catalysts. RSC Adv 2016. https://doi.org/10.1039/C6RA20450C.
[32] Usman M, WanDaud WMA, Abbas HF. Dry reforming of methane: influence of process parameters—a review. Renew Sustain Energy Rev 2015;45:710–44.
[33] Moon DK, Kim YH, Ahn H, Lee CH. Pressure swing adsorption process for recovering H_2 from the effluent gas of a melting incinerator. Ind Eng Chem Res 2014;53:15447–55.
[34] Liu K, Song C, Subramani V. Hydrogen and syngas production and purification technologies. New Jersey: Wiley; 2010.
[35] Chou CT, Chen FH, Huang YJ, Yang HS. Carbon dioxide capture and hydrogen purification from synthesis gas by pressure swing adsorption. Chem Eng Trans 2013;32:1855–60.
[36] Yang SL, Choi DY, Jang SC, Kim SH, Choi DK. Hydrogen separation by multi-bed pressure swing adsorption of synthesis gas. Adsorption 2008;14:583–90.
[37] Li B, He G, Jiang X, Dai Y, Ruan X. Pressure swing adsorption/membrane hybrid processes for hydrogen purification with a high recovery. Front Chem Sci Eng 2016. https://doi.org/10.1007/s11705-016-1567-1.
[38] Reddy S, Vyas S. Recovery of carbon dioxide and hydrogen from PSA tail gas. Energy Procedia 2009;1:149–54.
[39] Brea P, Delgado JA, Águeda VI, Uguina MA. Modeling of breakthrough curves of N_2, CH_4, CO, CO_2 and a SMR type off gas mixture on a fixed bed of BPL activated carbon. Separ Purif Technol 2017;179:61–71.
[40] Golden TC, Sircar S. Gas adsorption on silicalite. J Colloid Interface Sci 1994;162:182–8.
[41] Agueda VI, Delgado JA, Uguina MA, Brea P, Spjelkavik AI, Blom R, Grande C. Adsorption and diffusion of H_2, N_2, CO, CH_4 and CO_2 in UTSA-16 metal-organic framework extrudates. Chem Eng Sci 2015;124:159–69.
[42] Brea P, Delgado JA, Águeda VI, Uguina MA. Comparison between MOF UTSA-16 and BPL activated carbon in hydrogen purification by PSA. Chem Eng J 2019;355:279–89.
[43] Park JH, Kim JN, Cho SH, Kim JD, Yang RT. Adsorber dynamics and optimal design of layered beds for multicomponent gas adsorption. Chem Eng Sci 1998;53:3951–63.
[44] Park JH, Kim JN, Cho SH. Performance analysis of four-bed H_2 PSA process using layered beds. AIChE J 2000;46:790–802.
[45] Sircar S, Waldron WE, Rao MB, Anand M. Hydrogen production by hybrid SMR–PSA–SSF membrane system. Separ Purif Technol 1999;17:11–20.
[46] Grande CA, Blom R. Utilization of dual-PSA technology for natural gas upgrading and integrated CO_2 capture. Energy Procedia 2012;26:2–4.
[47] Jiang Y, Ling J, Xiao P, He Y, Zhao Q, Chu Z, Liu Y, Li Z, Webley PA. Simultaneous biogas purification and CO_2 capture by vacuum swing adsorption using zeolite NaUSY. Chem Eng J 2018;334:2593–602.
[48] Fuderer A, Rudelstorfer E. Selective adsorption process. 1976. US Patent 3986849.
[49] Hindmarsh AC. Serial Fortran Solvers for ODE Initial Value Problems. http://computation.llnl.gov/casc/odepack/odepack_home.html. accessed in January 2019.
[50] Effendy S, Xu C, Farooq S. Optimization of a pressure swing adsorption process for nitrogen rejection from natural gas. Ind Eng Chem Res 2017;56:5417–31.
[51] Park J, Lively RP, Sholl DS. Establishing upper bounds on CO_2 swing capacity in sub-ambient pressure swing adsorption via molecular simulation of metal–organic frameworks. J Mater Chem 2017;5:12258–65.
[52] Kuah WC, Effendy S, Farooq S. Industrial scale propylene/propane separation using pressure vacuum swing adsorption. Ind Eng Chem Res 2018;57:6451–63.
[53] Grande CA, Poplow F, Rodrigues AE. Vacuum pressure swing adsorption to produce polymer-grade propylene. Separ Sci Technol 2010;45:1252–9.
[54] Joss L, Hefti M, Bjelobrk Z, Mazzotti M. On the potential of phase-change adsorbents for CO_2 capture by temperature swing adsorption. Energy Procedia 2017;114:2271–8.
[55] Dinh DK, Choi S, Lee DH, Jo S, Kim KT, Song YH. Energy efficient dry reforming process using low temperature arcs. Plasma Process Polym 2018;15:e1700203.
[56] Bartholomew CH. Mechanisms of catalyst deactivation. Appl Catal Gen 2001;212:17–60.
[57] Gomes PS, Minceva M, Rodrigues AE. Simulated moving bed technology: old and new. Adsorption 2006;12:375–92.
[58] https://www.nrel.gov/docs/fy02osti/32405b2.pdf. accessed in January 2020.
[59] https://www.alibaba.com/showroom/activated-carbon-price-per-ton.html. accessed in January 2020.
[60] Pei P, Korom SF, Ling K, Nasah J. Cost comparison of syngas production from natural gas conversion and underground coal gasification. Mitig Adapt Strategies Glob Change 2016;21:629–43.